Impact of Acidalia Strom Track (AST) in Martian Atmosphere During MY 33 and 34:

A Case Study Over Kasei Valles

Jyotirmoy Kalita* and Anirban Guha
Department of Physics, Tripura University,
Suryamaninagar, Tripura, India

***Abstract*— Martian storms can potentially impact the lower/upper atmospheres through dust aerosol radiative heating/cooling and atmospheric circulation. Notably, the planet-encircling dust storm is the most dynamic phenomenon that substantially alters the temperatures and circulation patterns of the Martian atmosphere. Here we present the attempt to investigate how the dust impact transfers from the neutral upper atmosphere to the ionosphere over the Acidalia Strom Track (AST) passes through the largest liquid flow channel of Mars. Our results show that the main ionospheric layer (below ~250 km altitude) undergoes an overall upwelling or enhancement. Our analysis shows that during the dust storm season, ionosphere density varies from $1.8x10^6$ cm^{-3} to $5x10^6$ cm^{-3} at the height of ~150 to 170 km, and during non-dust storm season, it varies from $1.3x10^5$ cm^{-3} to $9x10^5$ cm^{-3} at a height of 100 to 120 km, much less than dust storm season. Further, the impact of regional and global dust storms is determined by accounting for predictable sources of ionospheric variability like EUV Flux, SZA, and neutral densities. This study suggests that significant dust activity can cause disturbances in ionospheric densities as well as upwelling of the ionospheric layer. These disturbances are tied to perturbations in the thermosphere caused by aerosol heating of atmospheric dust. The expansions of the atmosphere during the dust storms and the solar wind electron precipitation are considered plausible mechanisms for explaining the observed results. The effects of the lower atmospheric dust storms on the altitude of the Martian ionosphere are studied using a topside radar sounder (MARSIS) aboard the Mars Express spacecraft. For this purpose, we considered oblique echoes observed during Martian years 33 and 34. Our results consistently indicate that the altitude of the Martian ionosphere is higher during the dust storm period than before the onset of the dust storm. Also, we tried to investigate and verify the compositional variation of the Martian ionosphere during the Martian storms, using the ion density measurements made by the Neutral Gas and Ion Mass Spectrometer (NGIMS) onboard the Mars Atmosphere and Volatile Evolution. Also, we included the supportive evidence from MAVEN IUVS observed data for the mentioned events. At the height of 170 km, the variations of ionospheric species during the GDS show enhancement in CO2+, Ar+, H2O+ and depletion in O2+, O+, N2+/CO+ and OH+. These results will open a new window to study the atmosphere loss from the red planet.**

Keywords*— *Martian dust storm, Ionosphere, oblique echos, acidalia storm track.

INTRODUCTION

The escape of various gases from the Martian atmosphere from the primordial phase to date is a fascinated topic for the researcher. History of the presence of noble gases on Mars suggested that those gases could have evolved from primordial to present-day through two early episodes of hydrodynamic atmospheric escape [78]. In the first episode, escape of H_2 rich atmosphere in contact with Solar EUV and in the second episode, recycling of carbon isotopes leaving behind the noble gases with its isotopic composition [77]. The evolution of the Martian Atmosphere is one of the most fascinating problems in the exploration of our solar system [6,7,9,11,12]. Present-day, Mars has a very thin 6-millibar atmosphere in equilibrium with polar caps and regolith [51]. Both morphological and mineralogical evidence suggests that Martian Climate was warmer and wetter more than 3 billion years ago [31]. According to famous scientist HG Heaven, the Main mechanism for gas escape is thought to be Jeans escape of a steady hydrogen reservoir sourced from odd-oxygen reactions with near-surface water vapour [47,48]. Constraints on H loss have historically been made using hydrogen Lyman alpha (121.6 nm) light scattered in the planet's extended upper atmosphere or corona and for that scientists used the MAVEN-IUVS instrument to acquire the data [17,18,19,20]. Paramagnetic and superoxide form of oxygen reveals many windows to study the Martian atmosphere since the major part of the ionosphere is O2+ and recombination of O2+ usually occurs at the Martian exosphere [66] leading to the escape rate of water [14,15,16]. The neutral densities in this paper were obtained by the Neutral Gas and Ion Mass Spectrometer (NGIMS) on MAVEN, a quadrupole mass spectrometer that measures in situ densities in every orbit. NGIMS provides a unique opportunity to study upper atmospheric composition, as it has now measured densities between the nominal altitudes of approximately 150-350 km for over a full Martian year. This provides a large dataset for analysis of the neutral densities in the altitude regime where the atmosphere transitions from collisional to ballistic and neutral escape becomes more likely. Since ion precipitation is correlated with the direction of the solar wind convective electric field, it is more likely when the field is directed towards the planet [27,85,93]. In our present work, we are mainly interested to study the process of atmosphere escape from the Martian atmosphere. The present work basically put interest on the largest liquid flow channel of Mars, Kasei Valles [74,76]. We tried to see the effect of a dust storm near extremely low land. Further, we focused on the atmospheric parameter which definitely has strong contributions towards the atmospheric anomalies. Specifically, we want to concentrate on the effect of solar EUV and Dust storms (local as well as global) on the different layers of the

atmosphere over Kasei valles. The extension of the dust activity occurs in the red planet ranges from very small scale, i.e., dust devils, to very large-scale or planet-encircling dust storms (longitudinal axis >2000 km [63,64]. Many scientists put their efforts to understand the origin and circulation pattern of these dust storms [37,38]. Regional and Global dust storms last for more than a single Martian day or even for weeks and significantly put impact the atmospheric structure and circulation [22, 63, 64, 82, 88, 89, 90, 13, 84]. Haberle et al. (1982) and Wilson (1997) suggested that equatorward movement of dust storms injects dust into the rising branch of the Hadley circulation, hence they used to enhance the dust mixing into the upper atmosphere, and increase the mid-level air temperatures, which can be an indicator of dust storm occurrence. Also, regional dust storms help in the generation of a thick haze over many areas of the red planet that can reach up to an altitude of 60 km and increase the normal opacity by a huge factor [55, 56, 13,70]. Enhancement in the Martian Ionosphere is created regularly by solar X-ray and ultraviolet (UV) radiation and electron impact. On several occasions, many atmospheric parameters give inputs to the atmosphere of Mars and disturb its ionosphere leading to sudden enhancements in its density [44, 45, 60, 68]. Modelling studies have shown that dust storms can also cause ionization in the Martian atmosphere up to an altitude of ~80 km [44,45,14]. Moreover, dust storms may change the altitude of the ionospheric peak [92,68] due to the expansion of the Martian atmosphere as we mentioned while explaining the CBL height [88,61,89,90]. The Mars Advanced Radar for Subsurface and Ionospheric Sounding (MARSIS) regularly detects ionospheric bulges in the Martian ionosphere [5,28,29,40,41,86,87,71,75]. We reported a few cases in which peak frequencies of the oblique echo a greater than those of the vertical echoes and we further investigate causative mechanisms for the occurrence of such strong oblique echoes

DATA AND METHODOLOGY:

NGIMS data analysis:

Our present study uses the publicly available NGIMS level 2 data of October 2014, January 2016 and June 2018. NGIMS is a quadrupole mass spectrometer that measures in situ ion and neutral counts within a range of 2-150 amu. NGIMS has 1 amu resolution for each orbit. Both ion and neutral counts are measured by NGIMS in channels for mass-to-charge ratio in a 2.6 s cadence. The counts from each mass channel are converted to abundances in particles per cubic centimetre. The abundance is counted against the altitude, time, latitude, and longitude of the measurement in the instrument's level 2 data files. The present work estimates the changes in average neutral and ion density near the exobase during the dust event by comparing densities for species O, Ar, and CO2 in the 180-220 km altitude range. By looking at this altitude range, we can examine neutrals and ion density that might be enhanced by enhanced due to the dust event and temperature variance due to accumulation of dust particles over the area. Ar was chosen by the present work because it is chemically inert, meaning it does not undergo photochemical processes, while O and CO2 were chosen due to their dominance at the altitudes of interest i.e. below 250 km. For each orbit, we average the measured densities for each species over altitudes 180-220 km. The level 3 data is also analyzed to see the scale height of each component. Density bins are in logarithmic bins in level 3 data. Abundance generally referred to in the level 2 product is in part/cc. In the level 3 product, a resampled 'density' product is acquired in a 10km averaged bin. This is used to help smooth out each orbit and is useful for broader pictures of the atmosphere. It does smooth out wave features and is more useful for temperature profiles, but tends to lose the finer features from each orbit. The other L3 product (res-sht) computes the scale height and temperature using a fit to the log10 (abundance) vs altitude of the argon data. All positional information (altitude, solar zenith angle, local solar time, longitude, latitude, etc.) is computed using ephemeris data provided by spice kernels and is included in the level 2 data product.

MARSIS data analysis:

MARSIS data was analyzed by Rao et al shows that one may observe an enhancement of the ionosphere during or at the earlier stage of a dust storm. In our present work, we have three confirmed dust storm cases that are 2014, 2016 and 2018 for which we have analyzed the MARSIS data. MARSIS is a space-based radar sounder that is used to collect data in the nadir direction to probe the subsurface and ionospheric features of Mars [79]. It consists of a 40-m tip-to-tip dipole antenna that is used for transmitting high-frequency radio waves and thereby receiving the reflected echoes from the ionosphere, surface, and subsurface of Mars. In the active-ionospheric sounding mode of operation, it sweeps 160 frequencies between 0.1 and 5.5 MHz that are distributed quasi-logarithmically. The working principle for MARSIS during the active-ionospheric sounding mode of operation is illustrated in Kopf et al., 2008 [28,57]. When MARSIS transmits a frequency, reflections from ionized targets occur where the sounding frequency match with the local plasma frequency. Specular reflections occur when the iso-density surfaces are perpendicular to the transmitted rays. Instant sweeping from low frequency to high frequency, at first MARSIS receives reflections from higher altitudes with an increased frequency than from lower altitudes until the sounding frequency matches to the frequency of the main peak. When the sounding frequencies are higher than that reflected from the main peak, then we may say that reflections come from the surface of Mars. Each reflected frequency from the ionosphere corresponds to an electron density, which is given by the relation,

$$f_p = 8980\sqrt{n_e} \qquad (1)$$

where fp is the transmitted frequency in hertz and n_e is the electron density in per cubic centimetre. The "delay time" shown in figure 11, is often converted to "apparent altitude" with an assumption that the transmitted and reflected rays travel at the speed of light [1,40,57,72,73]. The highest frequency that reflects from the ionosphere is considered to be its main peak. Vertical lines in the ionogram in the bottom panel shown in Figure 4 represent the harmonics of electron plasma oscillations from which the electron density local to the

spacecraft can be obtained [29]. An ionospheric echo trace can also be estimated from the ionogram and with the combination of ionospheric echo and electron density local to the spacecraft can be inverted to get an electron density profile [1,40,57,72,73]. The presence of surface echoes and electron cyclotron echoes can also be noted in the ionogram. By measuring the separation between electron cyclotron echoes lines, the magnetic field information at the altitude of the spacecraft can be obtained which we will try for our next work under process [1,5,40]. It is to be mentioned that the separation between the vertical and oblique echoes indicates that the spacecraft is passing over an ionization bulge [1,40,57,72,73]

IUVS data Analysis:

Since the Lyman alpha line is optically thick so it is difficult to estimate the escape value and density from the intensity data of MAVEN-IUVS. So, we went back to 1970 to understand the forward model to calculate the intensity. Afterward we fitted the model intensity profile and original intensity profile to get the jeans escape value. In 1977 Anderson introduced the radiative transfer model assuming the corona to be isothermal, planetary line profile to be doppler and the solar lines are independent of frequency. Before Anderson and Hord, Chamberlin in 1963, tried to calculate the escape flux with the specified chemical composition, temperature and incident solar radiation. He found an escape rate of $6x10^6$ atom/cm^2 sec. Chamberlain also introduced the effect on the ionosphere which we have already discussed in or previous section with MARSIS data [21,22]. In the next year, Chamberlain forwarded the classic assumption of a sharply defined critical level (exobase), above which the atmosphere is completely free of collisions. Throughout, the different types of particle orbits are treated separately; coronal particles are either ballistic (meaning captive particles whose orbits intersect the critical level), satellite (captive particles orbiting above the critical level), or escaping. Liouville's equation leads to exact expressions for the density distributions and escapes flux [21,22]. After that, as we mentioned, Anderson introduces a new assumption of frequency redistribution and got an escape flux value of $2.4x10^{11}$ atom/cm^2 sec [2,3,4]. In 1999 Bishop tried to estimate the Lyman alpha and Lyman beta flux for which he got a value of $3.6x10^{11}$ atom/cm^{2}sec. In our present work, we closely follow the method used by Chaufray (2008) and Chaffin (2018).

Since Lyman alpha photons are multiply scattered in the Mars corona, so, a radiative transfer model is required to retrieve escape rates from intensity measurements. In our present work, we follow a forward modelling approach, coupling a parametric hydrogen density model to a photon scattering model introduced in previous literature [10,39,25]. Through this model we compute the brightness for a given model atmosphere, after that, we compared the data with observations. We also estimated the chi-squared difference of the data and the model data for minimum value and then fit the atmospheric parameters. We also follow the assumptions by the previous literature in both the density and radiative transfer modelling. As we mentioned earlier, the assumptions adopted in H coronal retrievals at Mars do not differ from the assumption followed in our present work [10,39,23,24,25] and these assumptions helped us to estimate a proper fit for the model data to observed coronal profiles. The density model we follow is identical to Chaufray et al. (2008). The model assumed a spherically symmetric atmosphere and accepts two parameters as input i.e. the number density and temperature of hydrogen at the exobase of the red planet. We assumed the exobase temperature to be at 200km. The complete procedure is mentioned in appendix III.

The second assumption is that the CO_2 density at 80 km is fixed to be 2.67×10^{13} cm−3 for all presented profiles, and the temperature of CO_2 is assumed identical to the H temperature. We consider the exobase at 200 km, so below exobase, we need to assume a density and temperature profile and for that, we consulted an analytic profile from Krasnopolsky (2002). This profile suggested a varying density profile of $9.5x10^5$ cm^{-3} to $3.5x10^6$ cm^{-3} in relation to a varying temperature profile of 100 to 150K below the exobase temperature. We also assumed the exosphere is assumed isothermal at the exobase temperature as assumed by Chaufray and Chaffin in their previous work. All velocity distributions are assumed to be Maxwellian at the temperature corresponding to the altitude for which the observational data are available. The CO_2 is assumed to have a hydrostatic density profile determined from the temperature-dependent scale height. We assumed the H density profile above the exobase contains the particle following ballistic orbits as mentioned for the Chamberlain exosphere [10,39,23,24,25]. We assumed the H density to be constant below 120 km. Since the atmosphere is mostly opaque for Lyman alpha the effect of the last assumption is negligible also, we mentioned the low altitude characteristics for the density and temperature profile based on Krasnopolsky et al., [10,39,23,24,25]. In brief, we assumed two parameters as input and tried with different combination for a particular height to minimize the chi-squared value and confirms our findings.

Starting from Anderson and Hord (1977) we went through Chamberlain (1962,1963) and ended up with Chaufray (2008), Bhattacharyya (2015,2016) and Chaffin (2018) to understand the complete assumption for the input of the forward model for radiative transfer. In addition, we also assume Gaussian line shapes and complete frequency redistribution to solve the radiative transfer equation. We consulted the precomputed atmospheric scattering on a grid of hydrogen density and temperature, resulting in source functions that are integrated along observation lines of sight for comparison with spacecraft measurements by Chaffin (Chaffin et al., 2018). the Jeans escape relationship for our calculation is given by,

$$\Phi = n\frac{V_{mp}}{2\pi^{\frac{1}{2}}}(1+\lambda)e^{-\lambda} \quad (2)$$

$$V_{mp} = \sqrt{\frac{2KT}{m}} \quad (3)$$

$$\lambda = \frac{GMm}{KTr_{exo}} \quad (4)$$

where ϕ is the exobase escape flux, n is the exobase density, T is the exobase temperature, V_{mp} is the most probable

Maxwell-Boltzmann velocity, λ is the escape or Jeans parameter, k is the Boltzmann constant, r(exo) is the exobase radius, m is the mass of the hydrogen atom, M is the planetary mass, and G is the universal gravitational constant.

Second this we need to know the χ^2-minimization technique to fit the data. $\chi 2$ is given as,

$$\chi^2(T_{exo}, n_{exo}) = \frac{1}{n-2}\sum_{i=1}^{n}\frac{(I_{o,i} - I_{m,i}(T_{exo}, n_{exo}))^2}{\sigma_{o.i}^2} \quad (5)$$

For each point of the refined grid defined by th parameters n_{exo}, T_{exo}, the quality of fit to the data is quantified by a value of $\chi 2$. Index I refer to the ith line of sight, Io is the observed intensity, Im the computed intensity, σo the standard deviation of the observed intensity and n is the number of lines of sight fitted for each orbit

RESULTS:

The present work first analysed the NGIMS data to see the neutral abundance in the Martian atmosphere. First, we analysed the neutral density during the 2018 GDS. Figure 1 represents the CO2 density during pre, ongoing and post dust storm scenarios. The present work tries to show the effect of the dust storm

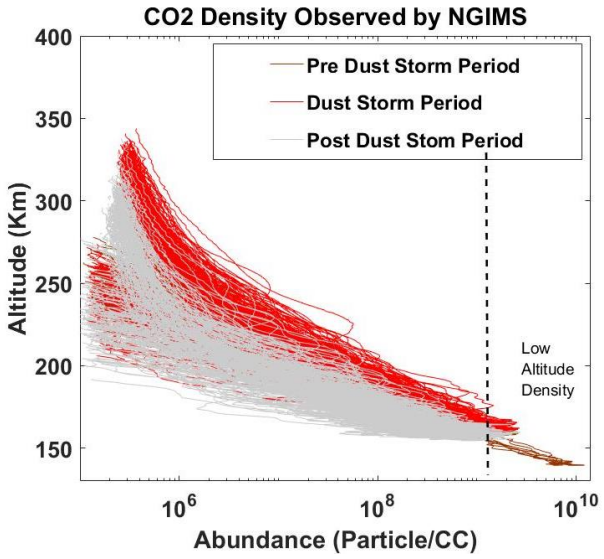

Figure 1: The figure illustrates the CO2 abundance during the 2018 GDS. We may see an enhancement in the neutral density during the global dust storm. Also, we may see the shifting of the maximum density layer during GDS. During the pre-dust storm period, lower atmosphere neutral density is higher.

The present work tries to see also the depletion of the ion during a global dust storm. We find that the hydroxyl ion gets depleted in the range of 10 power 2 during a global dust storm. That indicates the exospheric escape of water in the influence of EUV and UV. Also, we may see an oblique echo in MARSIS data due to the enhancement in the ionospheric density at the height of 170 to 200 Km. Also, we may see the upwelling of the ionospheric layer in the post dust storm season. The peak ionospheric layer went up to a height of 250km in the figure. Figure 2 illustrate the ion abundance during a dust storm along with the post and pre-dust storm season. There also, we may see an upwelling of the ion layer which further interact with the UV and FUV and get dissociate to escape the Martian exosphere.

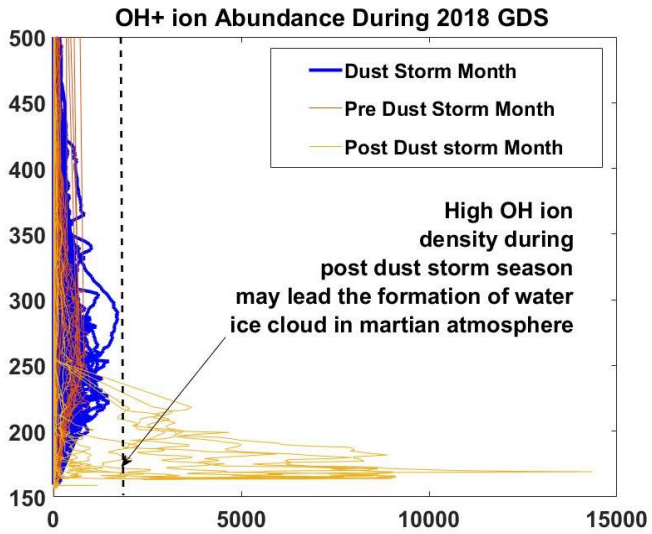

Figure 2: OH+ abundance during 2018 GDS along with pre and post dust storm month. We may clearly see the depletion of OH+ ion during a GDS which lead us to conclude the atmospheric escape process of Mars.

During 2014 RDS, accretion of dust we may see over the Kasei Valles. Deep convection activity is used to increase the lower atmosphere temperature due to which the CBL and scale height are used to increase for the species. It is to be mentioned that CBL decides the transportation of the species from the lower atmosphere to the upper atmosphere. For scale height data we consulted NGIMS level 3-res-sht publicly available product and matched with the previous literature based on satellite imagery. Figure 3 shows the ion abundance during the 2014 Regional Dust Storm (RDS). [49,50,51,52]. Scale height varies for CO2 from 8 to 10km.

The present work also tries to evaluate the same for the local dust storm observed during September 2016. We found significant enhancement in CO2+, Ar+, H2O+ and depletion in O2+, O+, N2+/CO+ and OH+. In figure 3 we showed the depletion of OH+ during a regional dust event.

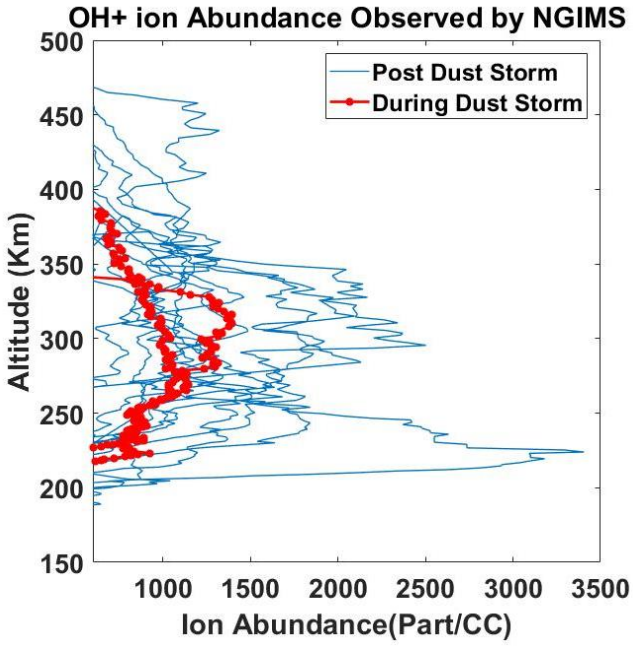

Figure 3: The figure illustrates the OH+ ion depletion during s regional dust storm. We may clearly see the scenario of ion abundance during and post dust storms.

Using observations of MARSIS instrument onboard the Mars Express spacecraft, we show the presence of unusually strong oblique echoes on Oct 2014 (Ls = 222°), September 2016 (Ls = 212°), June 2018 (Ls = 185°), The "unusually strong oblique echoes" are characterized by their peak densities, which are much greater than those of the vertical echoes and their peak altitudes which are much lower than that of the normal ionosphere. For 2016 and 2018 the echoes follow both the condition but for 2014 we may see the oblique echoes but with less peak density. The peak density in the first of these cases is ~1.98 × 10^5 cm^{-3} and was observed at an altitude of ~ 70 km from the mean surface of mars. In a subsequent case on 27 Oct 2014, the peak densities decreased and altitudes increased. These oblique echoes were observed in a region of relatively weak crustal magnetic fields between 15°S to 85°S latitudes and 39°N and 345°W longitudes, on which we need to focus our attention in our future works. There could be various mechanisms to enhance the ionosphere. In our present study, we consider only the dust events to be the only reason for ionospheric bulging and observed the effect accordingly. Reported density value was observed at a height of 70 to 90 km. Since we are working with MAVEN data using a forward model, we will have a rough idea about the density that we use as a parameter in the forward model to estimate the brightness of the layman alpha profile. Oblique echoes were also observed in other dust storm years though their peak frequencies are less than those observed in 2016. During all these years, the strong oblique echoes were not observed continuously throughout the dust storm period but only sporadically. At this point, it is important to remember the limitations of the MARSIS observing technique, which is a topside sounder. It cannot observe any ionization if its density is less than that of the main ionospheric layer (Rao et al.,2018). This means that even if there is dust enhanced ionization in the lower ionosphere, MARSIS will not be able to observe if its density is less than that of the main layer. Thus, MARSIS might have missed several important cases of enhanced ionization in the lower ionosphere. Interestingly we find the oblique echoes over weak magnetic fields also. One possibility is that the ionization is locally produced. In this case, the convection in the Martian dust storm transports the water vapour to these altitudes, which subsequently becomes atomic hydrogen [23,24] and gets ionized. That is why we consulted MAVEN-NGIMS data to see the water escape through photodissociation during a dust storm. In the lower atmosphere. Also, solar UV ionization plays a significant role in the ionization of dust aerosols. The deep convection in the dust storm makes the atmosphere expand which causes the upward movement of the neutrals and ions. As a result, the ionization due to dust aerosols moves to upper atmospheric altitudes. The process of deep convection involves both convective and advective motions that result in the complex movement of plasma. We know that during the Martian dust storms, turbocharging and altitude distribution of the aerosol particle sizes lead to large-scale electric fields [67,68,69]. During the early phase of the dust storm, the amount of ionization and electric fields created in the lower atmosphere may reduce because the UV radiation reaching the surface decreases and the mixing of dust aerosols increases. So, the upliftment and acceleration of aerosols from the lower atmosphere to the upper atmosphere happen more in the initial phases of the dust storm, and it decreases with an increase in dust activity. Such acceleration and transport of plasma in regions of open magnetic fields have been observed in the ionospheres and magnetospheres of several planetary bodies such as in the polar wind at Earth's high latitudes in the ionospheric holes at Venus and in the plasma plumes at Jupiter's moon Europa [8,46,26,53,54]. In situ measurements of neutral and ion compositions, temperatures, and electric fields are the most needed parameters to understand the acceleration processes that transport the plasma from the lower atmosphere to the ionospheric altitudes. From figure 11 we may see that the oblique echoes during 2014 and 2016 are much stronger than that of vertical echoes but in 2018 during the global dust storm the separation between the vertical and oblique echoes is increasing, hence the case is self-explanatory depending upon the above discussion. As we may see from the above discussion dust storms can lift the aerosol and boundary layer hence now, we sift our focus to find the effect of the dust storm afterwards

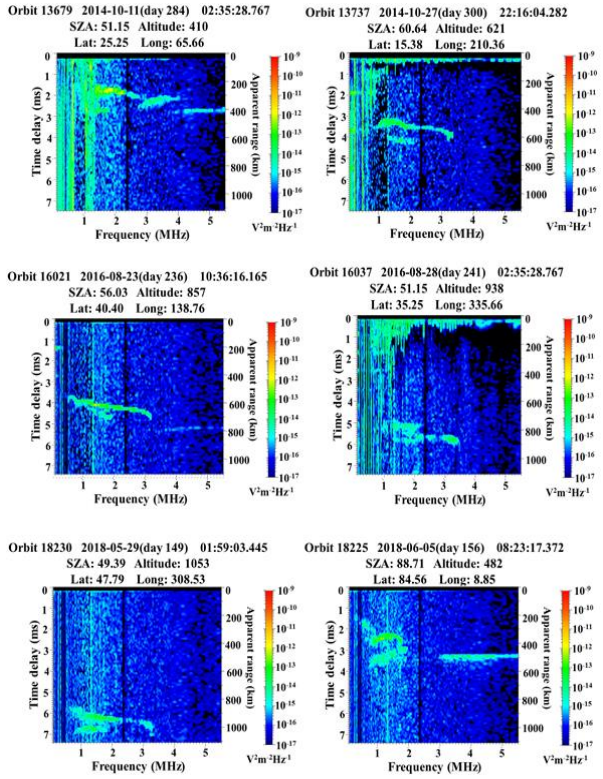

Figure 4: A series of ionograms for the years 2014,2016 and 2018. We may see the strong oblique echoes in all the ionogram indicates the time period before or during a local and global dust storm

After reaching the higher altitude, aerosols are encountered by high X and UV rays dissociate into its components and finally escaped the Martian atmosphere. Temperature and deep convection process play a major role in the process of dust storms [30,32,33,34,35,36,37,38] and in previous literature the escape process was reported as jeans escape/thermal escape process.

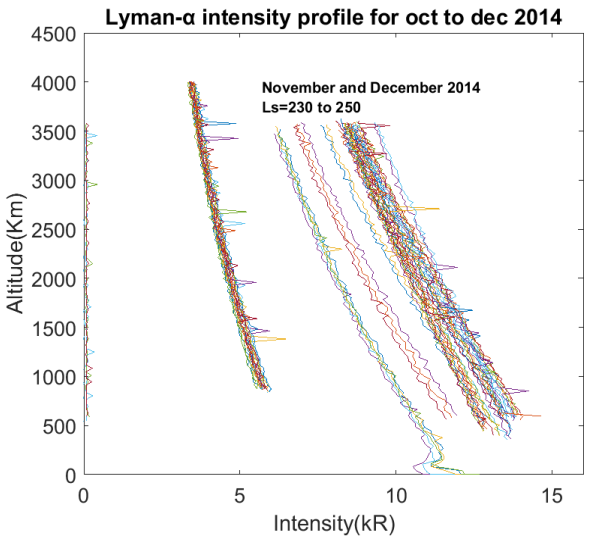

Figure 5: IUVS observed intensity for Lyman alpha line during the year 2014. During November and December, we may observe a high-intensity value indicated by the bunch of plots on the right-hand side.

We computed the escape flux for November and December using the forward model and we listed the value in table 1**:**

Table1: We furnished the exobase temperature, exobase density, and escape rate in the table.

Date	**Orbit**	**Ls**	**Exobase density (10^6 cm^{-3})**	**Maximum Intensity (kR)**	**Exobase temperature (K)**	**Thermal flux (10^8 cm^{-2}/s)**
29.12.2014	486	261.7	1.47	13.6199	195	8.82
12.11.2014	238	232	1.23	11.7261	187	7.72
11.10.2014	No data but from the colour plot, simulated model data gives an intensity of 12.34 kR, which in turn gives an escape flux of **$2.58x10^8$ cm^{-2}/s**					
21.10.2014	126	218.2	2.37	9.2385	205	10.21
28.10.2014	No data but from the colour plot, simulated model data gives an intensity of 7.34 kR, which in turn gives an escape flux of **$8.85x10^8$ cm^{-2}/s**					

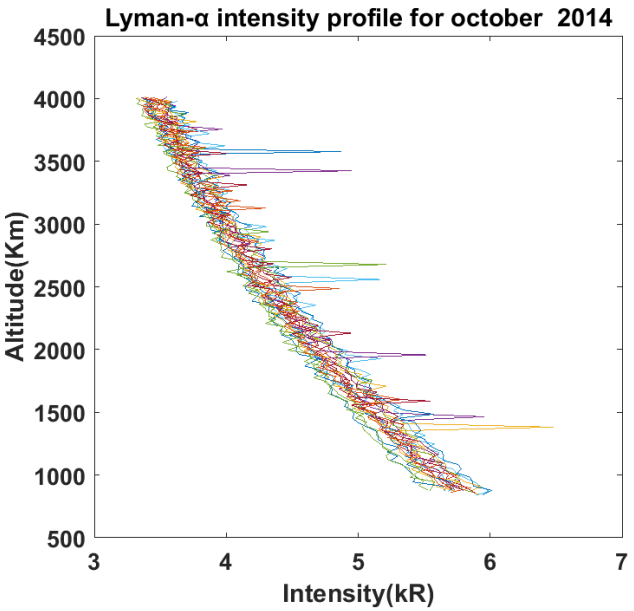

Figure 6: IUVS observed intensity for Lyman alpha line during early Oct 2014. We may see a maximum intensity of 6kR.

After we estimated the escape rate for 2014, we analyzed the 2015 data for MAVEN IUVS. Dust storm season start in mars from Ls=180, so we observe the intensity during a dust storm season for mars. Since late October, November and December 2014 we found the local dust storm and MARCI confirms the dust storm continuity through the earlier months of 2015 so with that deliberate intention we analyzed the data for 2015 also to give more rigidity to our results.

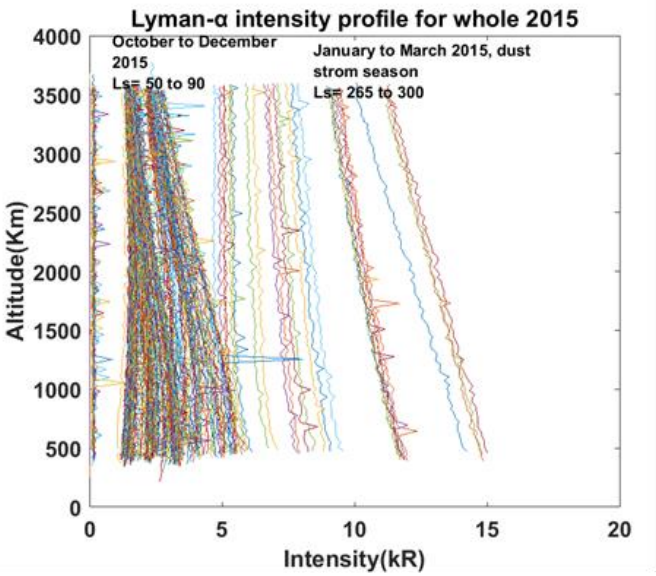

Figure 7: Intensity plot for the year 2015 for MAVEN-IUVS data. We separately indicate the intensity plots for two different seasons along with solar longitude.

We may clearly see from figure 7 that the intensity become higher during the earlier months of 2015 or during a dust storm season. he values of exobase temperature, density and escape rate for the year 2015. It is to be mentioned that during the earlier month of 2015 we got strong oblique echoes over the Hellas region with a strong crustal magnetic field which coincides with the result by Rao et al., 2018. A total of 305 days of data is available for 2015. To evaluate the escape rate we considered some criteria, i.e. the atmosphere is uniformly distributed and the particles follows the Maxwellian distribution. Since thin Lyman-α lines are difficult to analyze so we consulted the forward modeling to compare the model intensity with observed intensity. Through χ^2 minimization techniques we fitted the graph and estimated the escape rate (jeans escape). To be more accurate we consider the escape rate and exobase temperature as the input parameter in the forward model. The figure bellow shows a χ^2 value of 2.7 and an escape rate of 3.25×10^8 cm^{-3}/s with an exobase temperature of 220K and density is 0.6×10^6 cm^{-3}.

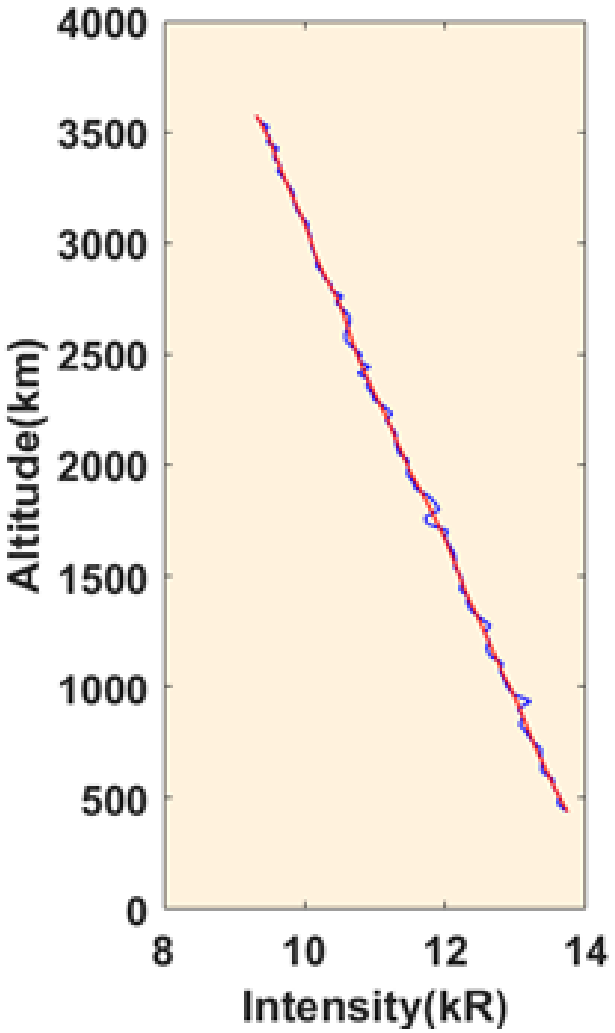

Figure 20: Model fit data (red curve) along with the observed intensity data (blue curve) where exobase is considered at 200 km.

During a dust storm, the escape rate is so high. So, we may say that the atmospheric water escape [58,59] is must faster on the red planet. Through the whole discussion, we put forward the dust distribution, the effect of a dust event in the various layer of the atmosphere so that we may easily predict the atmosphere escape for the red planet [80,81,83]. To understand properly the local atmosphere, we consider a few more events which we discussed date wise later in this section.

DISCUSSION:

The present work consulted satellite images that confirm 1 dust event/dust storm near Lunae Plenum and Kasei Valles during Dec 2014 [42,43]. We may see the structure of the dust event over the eastern side of the Kasei Valles (32°N/59°E) [91]. Deposition of dust and suspension of a dust particle in the Martian atmosphere blocked the solar incident radiation and we used to get a moderate albedo value. The temperature value varies from 220 to 240 K. The NGIMS data confirms the enhancement in the neutral as well as ion densities. Enhancement of the density confirms the uplift of neutral species and get dissociated in presence of UV and FUV. OH+ ion depleted during 2014 dust storm which indicates the

atmospheric chemistry involved in the escape of water into the Martian exosphere [62,65,66].

Before going to the MARSIS analysis, we need to see the MARCI daily weather report of Mars to know the location of our dust event. We consulted MARCI weekly report to predict the track of the dust event.

(http://www.msss.com/msss_images/2014/11/05/). On that week on Mars, a local scale dust storm was observed originating out of western Elysium tracking southward towards Gale Crater. After reaching and partially obscuring Gale Crater, the storm quickly abated. The Curiosity rover in Gale Crater experienced elevated levels of atmospheric opacity during that time. Amazonis and Cimmeria experienced local dust storms in the middle of the week. Local dust lifting events along the seasonal south polar ice cap generated a dust cloud over Aonia. Afternoon diffuse water-ice clouds were observed over Syria, southeast of Eos Chasma in Valles Marineras, and Arisa Mons, the southernmost volcano of the Tharsis Montes. Polar hood water-ice clouds continued to dip southward over the mid-latitude plains of Acidalia and Utopia. In figure 2 we may see the intense dust haze. The results of the present study show that there was a regional dust storm before and during the observation of the strong oblique echoes during 29 Dec 2014 with a peak density of 0.5x 106 cm-3. We estimated with a $\chi 2$ value of 1.4, the escape rate is ~8.8x108 cm-2/s with an exobase temperature of 240K and density is 1.47x106 cm-3. Our estimated value also coincides with MARSIS peak atmospheric density.

Maven-IUVS data shows an enhancement in the laymen alpha intensity. The present work also concludes that the uplift of hydroxyl ions occurs during the late phase of the dust storm. GDS is usually a strong event to carry the species up to the exosphere but regional dust storms follow a phase delay in this process. In figure 5 we may see that layman alpha intensity is 14 kr during the month of November instead of October.

2016 local and 2018 global dust storm:

MAVEN coronal scan data during the 2018 global dust storm is not available hence we only analyzed the NGIMS and MARSIS data for the present work. We may see the structure of the cloud/dust haze over the eastern side of the Kasei Valles (32°N/59°E) for 2016. We tried to find the reason for the occurrence of the dust haze and found a local dust storm over the Acidalia region (40° N). Further, we estimate the albedo value depending on the reactance value and found it to be varying from 0.8 to 0.9. Deposition of dust and suspension of a dust particle in the Martian atmosphere blocked the solar incident radiation and we used to get a high albedo value. Using albedo values, we calculated the approximate temperature. The temperature value varies from 200 to 240 K. The estimated temperature value indicates a favourable condition for the deep convection process. The upwelling of the ionospheric layer is confirmed by both NGIMS and MARSIS.

MARSIS data during and before the dust storm gave a peak density of 5x106cm-3. The most prominent two large regional dust storms were observed by MARCI over the northern hemisphere of Mars. The large arcuate-shaped dust storm, reported by MARCI, propagated eastward over the northern mid-latitudes of Utopia Planitia before abating. By midweek (30 September to 1 November 2015), a new dust storm had formed over the Ares III landing site. The dust storm moved southward along the Acidalia storm track into Xanthe Terra. By the end of the week, the storm covered an area from eastern Valles Marineris to north-central Arabia Terra, equivalent to the combined area of the entire United States and Mexico. More typical weather features were also spotted over the red planet. A number of local-scale dust storms occurred over northern Amazonis, Argyre, and Noachis Terra. Each afternoon, diffuse water-ice clouds were present over Tyrrhena Terra and the major shield volcanoes of Tharsis. In figure 4 we may observe the storm indicated by the red circle. A major regional-scale dust storm continued across Mars during November 2015. At the start of the week, the dust storm expanded along the northern hemisphere from eastern Tharsis to Elysium. Dust over Arabia was transported north of Syrtis along with the polar vortex, where it continued to spread eastward. During that time, the storm proliferated over the southern hemisphere, extending past the edge of the seasonal south polar ice cap, as far as the Mountains of Mitchel. By the end of the week, the storm stretched from Solis in the west to Cimmeria in the east, encompassing an area greater than 30 million square kilometres. Condensate water-ice clouds, typically observed above the major shield volcanoes of Tharsis, were absent during the second half of the week due to warmer atmospheric conditions caused by the storm. We analyzed the IUVS disk scan data and echelle mode data to see the intensity over the red planet during 2018. Estimated intensity values vary from 5.6 to 8 at the initial phase of the dust storm and during a dust storm and further, the intensity values increase up to 8.7 kR. But as far as the model and MCS temperature are concerned, we modelled the intensity to be >20kR. From this intensity value, we estimated the jeans escape flux value came out to be 2.865x109 cm-2/s with a temperature value that varies from 250 to 270K. So, we are waiting for the processed corona data to be available publicly to verify our findings. A huge amount of water was lost from the red planet during the global dust storm. NGIMS data confirm the enhancement and the depletion of the species during the global dust storm. We analyzed data for all the available species and found that GDS contribute in the enhancement in CO2+, Ar+, H2O+ and depletion in O2+, O+, N2+/CO+ and OH+. These results will open a new window to study the atmosphere loss from the red planet.

CONCLUDING REMARKS:

1. The observed dust storms occur in the Acidalia region. This dust storm track put influences the largest liquid flow channel of Mars. During 2014 both regional storms contribute to the dustiness over Kasei Valls. CBL and Scale height were used to increase during the dust storm near Kasei Valles.

2. Before and during the dust storm we find a strong oblique echo derived from MARSIS data indicates the presence of a deep convection process.

3. We estimated the maximum atmospheric density from MARSIS data to be 5x106 cm-3 at a height of ~80 km which also support further predicting the input parameter for MAVEN data analysis which helps us to know about the lower atmospheric scenario.

4. NGIMS data confirms the enhancement of the ion abundance and neutral species at the height of the ionosphere. Also, it shows enhancement of the ion abundance in the

exosphere which further support the escape of the planet atmosphere.

5. We analyzed the MAVEN-IUVS (all mode) data for 2014 to 2018 and found the escape rate varies from 6x107 cm-2/s to 2.4x109cm-2/s.

6. GDS influences instantly in the enhancement of the neutral and ion density and local/regional storm used to follow a phase delay. Also, we may see an upwelling of the ionospheric layer during and post dust storm period.

ACKNOWLEDGEMENT:

The authors are also thankful for the MCC data product team members for providing access to the required data for the present analysis (https://mrbrowse.issdc.gov.in/MOMLTA/) and the Indian Space Research Organization (ISRO) for funding the project with fund reference ISRO/SSPO/MOM-AO/2016-2019. A special thanks to Dr. Satadru Bhattacharya, Planetary Sciences Division, and Space Applications Centre (ISRO) for his constant support. The authors are thankful to Mr. Michael Chaffin, University of Colorado for his constant support in the analysis of MAVEN data. We are also thankful to MAVEN-IUVS team for the publicly available data in IUVS data are available on the Planetary Data System at http://atmos.nmsu.edu/ data_and_services/atmospheres data/ MAVEN/maven_iuvs.html. An acknowledgment is due to the Department of Science and Technology for a supporting fund to the Department of Physics, Tripura University through DST-FIST fund reference SR/FST/PSI-191/2014.

REFERENCES:

[1] Akalin, F., Morgan, D. D., Gurnett, D. A., Kirchner, D. L., Brain, D. A., Modolo, R., et al. (2010). Dayside induced magnetic field in the ionosphere of Mars. Icarus, 206(1), 104–111. https://doi.org/10.1016/j.icarus.2009.03.021

[2] Anderson, D. E., & Hord, C. W. (1977). Multidimensional radiative transfer: Applications to planetary coronae. Planetary and Space Science, 25(6), 563–571. https://doi.org/10.1016/0032-0633(77)90063-0

[3] Anderson, Jr. D. E. (1974). Mariner 6, 7, and 9 ultraviolet spectrometer experiment: Analysis of hydrogen Lyman alpha data. Journal Geophysical Research, 79, 1513–1518. https://doi.org/10.1029/JA079i010p01513

[4] Anderson, Jr. D. E., & Hord, C. W. (1971). Mariner 6 and 7 ultraviolet spectrometer experiment: Analysis of hydrogen Lyman-alpha data. Journal Geophysical Research, 76, 6666–6673. https://doi.org/10.1029/JA076i028p06666

[5] Andrews, D. J., André, M., Opgenoorth, H. J., Edberg, N. J. T., Diéval, C., Duru, F., et al. (2014). Oblique reflections in the Mars Express MARSIS data set: Stable density structures in the Martian ionosphere. Journal of Geophysical Research: Space Physics, 119, 3944–3960. https://doi.org/10.1002/2013JA019697

[6] Aoki, S., Vandaele, A. C., Daerden, F., Villanueva, G. L., Liuzzi, G., … Thomas, I. R. (2019). Water vapor vertical profiles on Mars in dust storms observed by TGO/NOMAD. Journal of Geophysical Research: Planets. doi:10.1029/2019je006109

[7] Arya, A. S., Sarkar, S. S., Srinivas, A. R., Manthira Moorthi, S., Patel, V. D., Singh, R. B., 2015. Mars Colour Camera: the payload characterization/calibration and data analysis from Earth imaging phase. Current Science. 109(06), 1076-1086. http://dx.doi.org/10.18520/cs/v109/i6/1076-1086

[8] Axford, W. I. (1968). The polar wind and the terrestrial helium budget. Journal of Geophysical Research, 73(21), 6855–6859. https://doi.org/10.1029/JA073i021p06855

[9] Benson, J. L., D. M. Kass, A. Kleinböhl, D. J. McCleese, J. T. Schofield, and F. W. Taylor 2010. Mars˝ south polar hood as observed by the Mars Climate Sounder. J. Geophys.Res., doi:10.1029/2009JE003554.

[10] Bhattacharyya, D., Clarke, J. T., Chaufray, J. Y., Mayyasi, M., Bertaux, J. L., Chaffin, M. S., … Villanueva, G. L. (2017). Seasonal Changes in Hydrogen Escape From Mars Through Analysis of HST Observations of the Martian Exosphere Near Perihelion. Journal of Geophysical Research: Space Physics, 122(11), 11,756–11,764. doi:10.1002/2017ja024572

[11] Braun, R. D., & Manning, R. M. (2007). Mars Exploration Entry, Descent, and Landing Challenges. Journal of Spacecraft and Rockets, 44(2), 310–323. doi:10.2514/1.25116

[12] Berman, D.C., Hartmann, W.K., 2002. Recent fluvial, volcanic and tectonic activity on the Cerberus plains of Mars. Icarus 159, 1–17.

[13] Cantor, B. A., 2007. MOC observations of 2001 planet encircling dust storm. Icarus, 186, 60-96.

[14] Cardnell, S., Witasse, O., Molina-Cuberos, G. J., Michael, M., Tripathi, S. N., Déprez, G., et al. (2016). A photochemical model of the dustloaded ionosphere of Mars. Journal of Geophysical Research: Planets, 121, 2335–2348. https://doi.org/10.1002/2016JE005077

[15] Carr, M. H. (1996). Water erosion on Mars and its biologic implications. Endeavour, 20(2), 56–60. doi:10.1016/0160-9327(96)10013-2

[16] Catling, David C.; Zahnle, Kevin J. (2009). "The Planetary Air Leak". Scientific American. 300 (5): 36–43. doi:10.1038/scientificamerican0509-36

[17] Chaffin, M. S., Chaufray, J. Y., Deighan, J., Schneider, N. M., Mayyasi, M., Clarke, J. T., Jakosky, B. M. (2018). Mars H Escape Rates Derived From MAVEN/IUVS Lyman Alpha Brightness Measurements and Their Dependence on Model Assumptions. Journal of Geophysical Research: Planets, 123(8), 2192–2210. doi:10.1029/2018je005574

[18] Chaffin, M. S., Chaufray, J. Y., Deighan, J., Schneider, N. M., McClintock, W. E., Stewart, A. I. F., Jakosky, B. M. (2015). Three-dimensional structure in the Mars H corona revealed by IUVS on MAVEN. Geophysical Research Letters, 42(21), 9001–9008. doi:10.1002/2015gl065287

[19] Chaffin, M.S., Chaufray, J.-Y., Stewart, I., Montmessin, F., Schneider, N.M., Bertaux, J.-L., 2014. Unexpected variability of Martian hydrogen escape. Geophys. Res. Lett.41, 314–320. doi:10.1002/2013GL058578.

[20] Chaffin, M.S., Chaufray, J.-Y., Stewart, I., Montmessin, F., Schneider, N.M., Bertaux, J.-L., 2014. Unexpected variability of Martian hydrogen escape. Geophys. Res. Lett.41, 314–320. doi:10.1002/2013GL058578.

[21] Chamberlain, J. W (1963). Planetary coronae and atmospheric evaporation. Planetary and Space Science, 11, 901. https://doi.org/10.1016/0032-0633(63)90122-3

[22] Clancy, R. T. et al., 2000. An intercomparison of ground- based millimeter, MGS TES, and Viking atmospheric temperature measurements: Seasonal and interannual variability of temperatures and dust loading in the global Mars atmosphere. J. Geophys. Res., 105(E4), 9553–9571.

[23] Clarke, J. T. (2018). Dust-enhanced water escape. Nature Astronomy, 2(2), 114–115. doi:10.1038/s41550-018-0383-6

[24] Clarke, J. T., Mayyasi, M., Bhattacharyya, D., Schneider, N. M., McClintock, W. E., Deighan, J. I., Jakosky, B. M. (2017). Variability of D and H in the Martian upper atmosphere observed with the MAVEN IUVS echelle channel. Journal of Geophysical Research: Space Physics. doi:10.1002/2016ja023479

[25] Clarke, J.T., Bertaux, J.-L., Chaufray, J.-Y., Gladstone, G.R., Quemerais, E., Wilson, J.K., Bhattacharyya, D., 2014. A rapid decrease of the hydrogen corona of Mars. Geophys. Res. Lett. 41, 8013–8020. doi:10.1002/2014GL061803.

[26] Collinson, G. A., McFadden, J., Grebowsky, J., Mitchell, D., Lillis, R., Withers, P., … Jakosky, B. (2020). Constantly forming sporadic E-like layers and rifts in the Martian ionosphere and their implications for Earth. Nature Astronomy. doi:10.1038/s41550-019-0984-8

[27] D. A. Brain, J. P. McFadden, J. S. Halekas, J. E P Connerney, S. W. Bougher, S. Curry, C. F.Dong, Y. Dong, F. Eparvier, X. Fang, K. Fortier, T. Hara, Y. Harada, B. M. Jakosky, R. J. Lillis, R. Livi, J. G. Luhmann, Y. Ma, R. Modolo, and K. Seki. The spatial distribution of planetary ion fluxes near Mars was observed by MAVEN. Geophysical Research Letters, 42(21):9142–9148, 2015.

[28] Diéval, C., Kopf, A. J., & Wild, J. A. (2018). Shapes of magnetically controlled electron density structures in the dayside Martian ionosphere. Journal of Geophysical Research: Space Physics, 123, 3919–3942. https://doi.org/10.1002/2017JA025140

[29] Duru, F., Gurnett, D. A., Averkamp, T. F., Kirchner, D. L., Huff, R. L., Persoon, A. M., et al. (2006). Magnetically controlled structures in the ionosphere of Mars. Journal of Geophysical Research, 111, A12204. https://doi.org/10.1029/2006JA011975

[30] Ehlmann, B. L., Mustard, J. F., Murchie, S. L., Bibring, J.-P., Meunier, A., Fraeman, A. A., & Langevin, Y. (2011). Subsurface water and clay mineral formation during the early history of Mars. Nature, 479(7371), 53–60. doi:10.1038/nature10582
[31] Fassett, C. I., & Head, J. W. (2011). Sequence and timing of conditions on early Mars. Icarus, 211(2), 1204–1214. doi: 10.1016/j.icarus.2010.11.014
[32] Fedorova, A. A., Montmessin, F., Korablev, O., Luginin, M., Trokhimovskiy, A., Belyaev, D. A., … Wilson, C. F. (2020). Stormy water on Mars: The distribution and saturation of atmospheric water during the dusty season. Science, eaay9522. doi:10.1126/science.aay9522
[33] Fedorova, A., Bertaux, J.-L., Betsis, D., Montmessin, F., Korablev, O., Maltagliati, L., & Clarke, J. (2018). Water vapor in the middle atmosphere of Mars during the 2007 global dust storm. Icarus, 300, 440–457. doi: 10.1016/j.icarus.2017.09.025
[34] Fisher, J. A., M. I. Richardson, C. E. Newman, et al., 2005. A survey of Martian dust devil activity Mars Global Surveyor Mars Orbital Camera images. Journal of geophysical research, 110, E03004, doi:10.1029/2003JE002165.
[35] Fonseca, R. M., Zorzano, M., & Martín-Torres, J. (2019). MARSWRF Prediction of Entry Descent Landing Profiles: Applications to Mars Exploration. Earth and Space Science, 6(8), 1440–1459. doi:10.1029/2019ea000575
[36] Forget, F., F. Hourdin, R. Fournier, C. Hourdin, O. Talagrand, M. Collins, S. R. Lewis, P. L. Read, and J. P. Huot, 1999. Improved general circulation models of the Martian atmosphere from the surface to above 80 km. J. Geophys. Res., 104, 24,155– 24,176.
[37] Gierasch, P.J. and R.M. Goody, 1973. A Model of a Martian Great Dust Storm. J. Atmos. Sci., 30, 169–179.
[38] Golitsyn, G. S., 1973. On the Martian dust storms. Icarus, 18, 113-119.
[39] Guha, B. K., Panda, J., & Chauhan, P. (2018). Analysing some Martian atmospheric characteristics associated with a dust storm over the Lunae Planum region during October 2014. Icarus. doi:10.1016/j.icarus.2018.09.018
[40] Gurnett, D. A., Huff, R. L., Morgan, D. D., Persoon, A. M., Averkamp, T. F., Kirchner, D. L., et al. (2008). An overview of radar soundings of the Martian ionosphere from the Mars Express' spacecraft. Advances in Space Research, 41(9), 1335–1346. https://doi.org/10.1016/j.asr.2007.01.062
[41] Gurnett, D. A., Kirchner, D. L., Huff, R. L., Morgan, D. D., Persoon, A. M., Averkamp, T. F., et al. (2005). Radar soundings of the ionosphere of Mars. Science, 310(5756), 1929–1933. https://doi.org/10.1126/science.1121868
[42] Guzewich, S.D. et al., 2015. Mars Orbiter Camera climatology of textured dust storms. Icarus 258, 1–13, doi.org/10.1016/j.icarus.2015.06.023.
[43] Guzewich, S.D. et al., 2017. An investigation of dust storms observed with the Mars Color Imager. Icarus, 289, 199–213, doi.org/10.1016/j.icarus.2017.02.020.
[44] Haider, S. A., Abdu, M. A., Batista, I. S., Sobral, J. H., Kallio, E., Maguire, W. C., & Verigin, M. I. (2009). On the responses to solar X-ray flare and coronal mass ejection in the ionospheres of Mars and Earth. Geophysical Research Letters, 36, L13104. https://doi.org/10.1029/ 2009GL038694
[45] Haider, S. A., Sheel, V., Smith, M. D., Maguire, W. C., & Molina-Cuberos, G. J. (2010). Effect of dust storms on the D region of the Martian ionosphere: Atmospheric electricity. Journal of Geophysical Research, 115, A12336. https://doi.org/10.1029/2010JA016125
[46] Hartle, R. E., & Grebowsky, J. M. (1990). Upward ion flow in ionospheric holes on Venus. Journal of Geophysical Research, 95(A1), 31–37. https://doi.org/10.1029/JA095iA01p00031
[47] Heavens, N. G., et al., 2011. The vertical distribution of dust in the Martian atmosphere during northern spring and summer: Observations by the Mars Climate Sounder and analysis of zonal average vertical dust profiles. J. Geophys. Res., 116, E04003, doi:10.1029/2010JE003691.
[48] Heavens, N. G., Kleinböhl, A., Chaffin, M. S., Halekas, J. S., Kass, D. M., Hayne, P. O., … Schofield, J. T. (2018). Hydrogen escape from Mars enhanced by deep convection in dust storms. Nature Astronomy, 2(2), 126–132. doi:10.1038/s41550-017-0353-4
[49] Hoekzema, N.M. et al., 2007. The scale-height of dust around Pavonis Mons from HRSC stereo images. In: Seventh International Conference on Mars, LPI Contributions No. 1353, p. 3154.
[50] Hoekzema, N.M. et al., 2010. Optical depth and its scale-height in Valles Marineris from HRSC stereo images. Earth Planet. Sci. Lett. 294, 534–540.
[51] Hu, R., Kass, D. M., Ehlmann, B. L., & Yung, Y. L. (2015). Tracing the fate of carbon and the atmospheric evolution of Mars. Nature Communications, 6(1). doi:10.1038/ncomms10003
[52] Hunten, D.M., 1973. The escape of light gases from planetary atmospheres. J. Atmos. Sci. 30, 1481–1494.
[53] Jakosky, B. M., Lin, R. P., Grebowsky, J. M., Luhmann, J. G., Mitchell, D. F., Beutelschies, G., Baird, D. (2015). The Mars Atmosphere and Volatile Evolution (MAVEN) Mission. Space Science Reviews, 195(1-4), 3–48. doi:10.1007/s11214-015-0139-x
[54] Jia, X., Kivelson, M. G., Khurana, K. K., & Kurth, W. S. (2018). Evidence of a plume on Europa from Galileo magnetic and plasma wave signatures. Nature Astronomy, 2(6), 459–464. https://doi.org/10.1038/s41550-018-0450-z
[55] Kleinböhl, A., et al., 2009. Mars Climate Sounder limb profile retrieval of atmospheric temperature, pressure, dust, and water ice opacity, J. Geophys. Res., 114, E10006, doi:10.1029/2009JE003358.
[56] Kleinböhl, A., et al., 2009. Mars Climate Sounder limb profile retrieval of atmospheric temperature, pressure, dust, and water ice opacity, J. Geophys. Res., 114, E10006, doi:10.1029/2009JE003358.
[57] Kopf, A. J., Gurnett, D. A., Morgan, D. D., & Kirchner, D. L. (2008). Transient layers in the topside ionosphere of Mars. Geophysical Research Letters, 35, L17102. https://doi.org/10.1029/2008GL034948
[58] Krasnopolsky, V. A. (2002). Mars' upper atmosphere and ionosphere at low, medium, and high solar activities: Implications for evolution of water. Journal Geophysical Research, 107, 5128. https://doi.org/10.1029/2001JE001809
[59] Krasnopolsky, V. A. (2015). Variations of the HDO/H2O ratio in the Martian atmosphere and loss of water from Mars. Icarus, 257, 377–386. https://doi.org/10.1016/j.icarus.2015.05.021
[60] Lee, C. O., Jakosky, B. M., Luhmann, J. G., Brain, D. A., Mays, M. L., Hassler, D. M., et al. (2018). Observations and impacts of the10 September 2017 solar events atMars: An overview and synthesis of the initial results. Geophysical Research Letters, 45, 8871–8885. https://doi.org/10.1029/2018GL079162
[61] Liuzzi, G., Villanueva, G. L., Crismani, M. M. J., Smith, M. D., Mumma, M. J., Daerden, F., … Patel, M. R. (2020). Strong Variability of Martian Water Ice Clouds During Dust Storms Revealed From ExoMars Trace Gas Orbiter/NOMAD. Journal of Geophysical Research: Planets, 125(4). doi:10.1029/2019je006250
[62] Lundin, R., Winningham, D., Barabash, S., Frahm, R. A., Andersson, H., Holmström, M., Bochsler, P. (2006). Ionospheric plasma acceleration at Mars: ASPERA-3 results. Icarus, 182(2), 308–319. doi:10.1016/j.icarus.2005.10.035
[63] Martin, L. J., and R. W. Zurek, 1993. An analysis of the history of dust activity on Mars. J. Geophys. Res., 98(E2), 3221–3246.
[64] Martin, T.Z., M. I. Richardson, 1993. New dust opacity mapping from Viking Infrared Thermal Mapper data. J. Geophys. Res., 98, 10, http://dx.doi.org/10.1029/93JE01044.
[65] McCleese, D. J., et al, 2007. Mars Climate Sounder: An investigation of thermal and wate vapor structure, dust and condensate distributions in the atmosphere, and energy balance of the polar regions, J. Geophys. Res., 112, E05S06, doi:10.1029/2006JE002790.
[66] McElroy, M. B., Kong, T. Y., & Yung, Y. L. (1977). Photochemistry and evolution of Mars' atmosphere: A Viking perspective. Journal of Geophysical Research, 82(28), 4379–4388. doi:10.1029/js082i028p04379
[67] Melnik, O., & Parrot, M. (1998). Electrostatic discharge in Martian dust storms. Journal of Geophysical Research, 103(A12), 29,107–29,117. https://doi.org/10.1029/98JA01954
[68] Mendillo, M., Withers, P., Hinson, D., Rishbeth, H., & Reinisch, B. (2006). Effects of solar flares on the ionosphere of Mars. Science, 311(5764), 1135–1138. https://doi.org/10.1126/science.1122099
[69] Michaels, T. I., and S. C. R. Rafkin, 2004. Large eddy simulation of atmospheric convection on Mars. Q.J.R Meteorol. Soc., 130, 1251–1274, doi:10.1256/qj.02.169.
[70] Mishra, M. K., P. Chauhan, R. Singh, S. M. Moorthi, and S. S. Sarkar, 2016. Estimation of dust variability and scale height of Atmospheric Optical Depth (AOD) in the Valles Marineris on Mars by Indian Mars Orbiter Mission (MOM) data. Icarus, 265, 84-94.
[71] Mohanamanasa, P., Venkateswara Rao, N., Yaswanth, C., & Rao, S. V. B. (2018). Magnetically controlled density structures in the Martian ionosphere: Are they stably recurring? Journal of Geophysical Research: Space Physics, 123, 5790–5806. https://doi.org/10.1029/2017JA024920

[72] Morgan, D. D., Gurnett, D. A., Kirchner, D. L., Fox, J. L., Nielsen, E., & Plaut, J. J. (2008). Variation of the Martianionospheric electron density from Mars Express radar soundings. Journal of Geophysical Research, 113, A09303. https://doi.org/10.1029/2008JA013313
[73] Morgan, D. D., Gurnett, D. A., Kirchner, D. L., Huff, R. L., Brain, D. A., Boynton, W. V., et al. (2006). Solar control of radar wave absorption by the Martian ionosphere. Geophysical Research Letters, 33, L13202. https://doi.org/10.1029/2006GL026637
[74] Muriel Gargaud, Encyclopaedia of Astrobiology, Volume 3, Springer Science & Business Media, May 26, 2011, p. 879.
[75] Nielsen, E., Fraenz, M., Zou, H., Wang, J. S., Gurnett, D. A., Kirchner, D. L., et al. (2007). Local plasma processes and enhanced electron densities in the lower ionosphere in magnetic cusp regions on Mars. Planetary and Space Science, 55(14), 2164–2172. https://doi.org/10.1016/j.pss.2007.07.003
[76] Orosei, R., Lauro, S. E., Pettinelli, E., Cicchetti, A., Coradini, M., Cosciotti, B., Seu, R. (2018). Radar evidence of subglacial liquid water on Mars. Science, eaar7268. doi:10.1126/science. aar7268
[77] Pepin, R. (1994). Evolution of the Martian Atmosphere. Icarus, 111(2), 289–304. doi:10.1006/icar.1994.1146
[78] Pepin, R. O. (1991). On the origin and early evolution of terrestrial planet atmospheres and meteoritic volatiles. Icarus, 92(1), 2–79. doi:10.1016/0019-1035(91)90036-s
[79] Picardi, G., Biccari, D., Seu, R., Plaut, J., Johnson, W. T. K., Jordan, R. L., et al. (2004). In A. Wilson (Ed.), Mars Express: A European Mission to the Red Planet, ESA Rep. SP-1240 (pp. 51–69). Noordwijk, Netherlands: European Space Agency Publ., Division.
[80] R. Gabriel Joseph, Regina S. Dass, V. Rizzo, N. Cantasano, G. Bianciardi. (2019). Evidence of Life on Mars?. Journal of Astrobiology and Space Science Reviews, Vol 1, 40-81, 2019.
[81] Rafkin, S. C. R., 2009. A positive radiative-dynamic feedback mechanism for the maintenance and growth of Martian dust storms. J. Geophys. Res., 114, E01009, doi:10.1029/2008JE003217.
[82] Smith, M.D., 2002. The annual cycle of water vapor on Mars as observed by the thermal emission spectrometer. J. Geophys. Res. 107, 5115, doi.org/10.1029/2001JE001522.
[83] Spiga, A., F. Forget, S. R. Lewis, and D. Hinson, 2010. Structure and dynamics of the convective boundary layer on Mars as inferred from large-eddy simulations and remote sensing measurements. Q. J. R. Meteorol. Soc., 136: 414–428. DOI:10.1002/qj.563.
[84] Strausberg, M. J., H. Wang, M. I. Richardson, S. Ewald, A. D. Toigo, 2005. Observations of the initiation and evolution of the 2001 Mars global dust storm. J. Geophys. Res., 110 (E2).
[85] Takuya Hara, Janet G Luhmann, François Leblanc, Shannon M Curry, Kanako Seki, David ABrain, Jasper S Halekas, Yuki Harada, James P. McFadden, Roberto Livi, Gina A. DiBraccio, John E P Connerney, and Bruce M Jakosky. MAVEN observations on a hemispheric asymmetry of precipitating ions toward the Martian upper atmosphere according to the upstream solar wind electric field. Journal of Geophysical Research: Space Physics, pages1–19, 2017.
[86] Venkateswara Rao, N., ManasaMohana, P., Jayaraman, A., & Rao, S. V. B. (2016). Some new aspects of the transient ionization layer of comet Siding Spring origin in the Martian upper atmosphere. Journal of Geophysical Research: Space Physics, 121, 3592–3602. https://doi.org/10.1002/2015JA022189
[87] Venkateswara Rao, N., Mohanamanasa, P., & Rao, S. V. B. (2017). Magnetically controlled density structures in the topside layer of the Martian ionosphere. Journal of Geophysical Research: Space Physics, 122, 5619–5629. https://doi.org/10.1002/2016JA023545
[88] Wang, H., 2007. Dust storms originating in the northern hemisphere during the third mapping year of Mars Global Surveyor. Icarus, 189, 325–343, doi:10.1016/j.icarus.2007.01.014.
[89] Wang, H., M. I. Richardson, R. J. Wilson, A. P. Ingersoll, and R. W. Zurek, 2003. Cyclones, Tides, and the Origin of Major Dust Storms on Mars. Geophys. Res. Lett., 30, 9, 1488. Doi:10.1029/2002GL016828.
[90] Wang, J.-S., & Nielsen, E. (2003). Behavior of the Martian dayside electron density peak during global dust storms. Planetary and Space Science, 51(4-5), 329–338. https://doi.org/10.1016/S0032-0633(03)00015-1
[91] Williams, R. M., Phillips, R. J., & Malin, M. C. (2000). Flow rates and duration within Kasei Valles, Mars: Implications for the formation of a Martian Ocean. Geophysical Research Letters, 27(7), 1073–1076. doi:10.1029/1999gl010957
[92] Withers, P., Weiner, S., & Ferreri, N. R. (2015). Recovery and validation of Mars ionospheric electron density profiles from Mariner 9. Earth, Planets and Space, 67, 194. https://doi.org/10.1186/s40623-015-0364-2
[93] Xiaohua Fang, Stephen W. Bougher, Robert E. Johnson, Janet G. Luhmann, Yingjuan Ma, Yung-Ching Wang, and Michael W. Liemohn. The importance of pickup oxygen ion precipitation to the Mars upper atmosphere under extreme solar wind conditions. Geophysical Research Letters, 40(10):1922–1927, may 2013.